# Novel Tulip-Shaped Three-body Orbits for Cislunar Space Domain Awareness Missions

**Darin C. Koblick**
*Raytheon*

## ABSTRACT

New families of quasi-periodic tulip-shaped orbits, derived from forking a near rectilinear halo orbit (NRHO) around the second Earth-Moon Lagrange point, are independently discovered and presented for the first time in scientific literature. Characterized by their nearly symmetric lobes, periods spanning 12 to 26 earth-days, and low perilune altitudes suitable for near-surface fly-bys, these orbits are similar to NRHOs but distinguishable by their quasi-periodic nature and variable apolune and perilune altitudes. This variability makes them advantageous for tracking, surveillance, communication, and navigation missions requiring geometric measurement diversity. These novel quasi-periodic orbits are compared against more traditional three-body cislunar trajectories such as NRHOs and butterfly orbits for lunar surface monitoring and space domain awareness (SDA) missions using standard catalog coverage metrics such as gap times. A comparative analysis was performed with a cislunar target catalog, consisting of 15 targets across eight orbit families, and 64 surface target locations from the NASA catalog of man-made material on the moon. Findings demonstrate that average minimum and maximum gap times decrease with an increase in lobes.

## 1. INTRODUCTION

Following Poincaré's seminal 1892 publication, the three-body problem sparked significant interest to the mathematical and scientific communities [1]. Early investigations focused on solutions to the planar problem and identified a number of different periodic orbit families. By 1920 some periodic orbits were generated from infinitesimal periodic oscillations but calculations relied upon analytical approximations near equilibrium points making it practically impossible to determine arbitrary three-dimensional solutions [2].

One intriguing aspect in finding periodic solutions is in its application to astrodynamics and Space Domain Awareness (SDA) communities. A common theme within the astrodynamics community has been to organize, classify, and store a variety of periodic solutions, as well as the required methodology to numerically produce them [3]. This cataloging effort supports mission designers by offering a variety of orbit candidates for the construction of deep-space and cislunar mission trajectories. More recently, the stability and flow to these orbits has become critical to evaluating periodic solutions. Stable and unstable manifolds, which exist near a periodic orbit, can be used as the foundation for low-energy transfer pathways. These manifolds allow for a spacecraft to arrive at, or depart from, periodic orbits with a minimal amount of $\Delta V$. Independent trajectory arcs can be combined to produce initial trajectory designs for interplanetary missions.

In previous work performed by Davis et al [4], several unique "quasi-periodic tulip-shaped orbits" about the Earth-Moon system were discovered by adding certain velocity perturbations to an NRHO within the lunar vicinity. Three years prior, the same researchers found a six petal tulip-shaped orbit around Saturn's largest moon, Titan, with 2D Poincaré maps [5]. Both papers cited a clear need for further investigation sparking interest in this research to discover, catalog and present a methodology to produce different families of tulip-shaped periodic orbits within the context of the classic three-body problem. To date, this research represents the most extensive examination of this particular peridoic orbit family.

The following outline overviews the structure of this paper. Section 2 introduces the classical simplified three-body dynamics model followed by a common approach to finding co-linear periodic orbits via linearized system of equations. The construction of an NRHO from a third order analytic halo orbit is provided followed by the discovery of fifteen families of tulip-shaped periodic orbits and their corresponding initial dimensionless states in section 3. Hodographs of the Jacobi constant and stability index vs perilune altitude are presented for each family along with selected trajectories after an ephemeris transition via DE 421 lunar ephemeris. Coverage metrics, discussed in previous SDA studies are outlined in section 4 along with a target catalog consisting of fifteen cislunar target trajectories and 64 surface targets from NASA's catalog of man-made material on the moon. A thousand trial Monte Carlo simulation is performed for each tulip-shaped orbit family to assess gap time performance in section 5. Section 6 discusses conclusions and additional areas of research followed by an appendix which provides a variety of three-dimensional tulip-shaped orbits for each newly discovered family.

## 2. THEORY

### 2.1 Simplified Dynamical Model

The well known Circular Restricted Three Body Problem (CR3BP) describes the dynamics of a spacecraft affected by two primary gravitational bodies, $P_1$ and $P_2$ [6]. It is assumed that the primary bodies are orbiting a common center of mass in circular orbits and unaffected by the spacecraft ($P_3$). The spacecraft will therefore move freely under the gravitational influence of $P_1$ and $P_2$ such that

$$\ddot{x} = \frac{\partial U}{\partial x} + 2\dot{y}, \quad \ddot{y} = \frac{\partial U}{\partial y} - 2\dot{x}, \quad \ddot{z} = \frac{\partial U}{\partial z}, \tag{1}$$

where the pseudopotential, $U$, is defined as

$$U = \frac{1}{2}\left(x^2 + y^2\right) + \frac{1-\mu}{d} + \frac{\mu}{r}, \tag{2}$$

the cartesian position and velocity components of the spacecraft with respect to the synodic frame, $\mathbf{X} = \begin{bmatrix} x & y & z & \dot{x} & \dot{y} & \dot{z} \end{bmatrix}^T$, $d = |P_3 - P_1|$, $r = |P_3 - P_2|$, and the mass ratio of the system, $\mu = m_2/(m_1 + m_2)$, is found assuming that $m_2 < m_1$. These dynamics allow for an integral of motion to exist, the Jacobi constant,

$$J = 2U - \left(\dot{x}^2 + \dot{y}^2 + \dot{z}^2\right). \tag{3}$$

The boundary of possible motion for a spacecraft with a particular Jacobi constant can be computed by setting the velocity of the spacecraft equal to zero, also known as a zero velocity curve. This is useful in finding forbidden regions, places a spacecraft cannot directly access, as J can never increase from imparting velocity into the system.

The differential equation for the State Transition Matrix (STM), $\Phi(t,0)$ , a matrix of partial derivatives, $\partial\mathbf{X}(t)/\partial\mathbf{X}(0)$, associated with the CR3BP dynamics is

$$\dot{\Phi}(t,0) = F(t)\Phi(t,0), \tag{4}$$

where $F(t) = \partial\dot{\mathbf{X}}(t)/\partial\mathbf{X}(t)$ is equal to

$$F(t) = \begin{bmatrix} 0_{3\times3} & I \\ U_{XX} & 2\Omega \end{bmatrix}, \ I = \begin{bmatrix} 1 & 0 & 0 \\ 0 & 1 & 0 \\ 0 & 0 & 1 \end{bmatrix}, \ \Omega = \begin{bmatrix} 0 & 1 & 0 \\ -1 & 0 & 0 \\ 0 & 0 & 0 \end{bmatrix}, \ U_{XX} = \begin{bmatrix} \partial\ddot{x}/\partial x & \partial\ddot{x}/\partial y & \partial\ddot{x}/\partial z \\ \partial\ddot{y}/\partial x & \partial\ddot{y}/\partial y & \partial\ddot{y}/\partial z \\ \partial\ddot{z}/\partial x & \partial\ddot{z}/\partial y & \partial\ddot{z}/\partial z \end{bmatrix} \tag{5}$$

### 2.2 Stability Index

One useful metric for mission designers is orbital stability, this can be represented in terms of a stability index [7]

$$\nu = \frac{1}{2}\left(|\lambda_{max}| + \frac{1}{|\lambda_{max}|}\right) \tag{6}$$

where $\lambda_{max}$ is the maximum eigenvalue of the monodromy matrix, $M$, computed by propagating the STM forward one orbital period, $M = \Phi(T,0)$.

The stability index, $\nu$, determines how fast invariant manifolds approach or depart the orbit [3], the larger the size magnitude, the faster the manifolds approach or depart from the orbit. A small stability index reflects slow departures from the orbit and is therefore related to lower station keeping requirements.

- If $\nu \leqslant 1$ then the orbit is marginally stable and eigenvectors will not yield stable and unstable invariant manifolds. These orbits are excellent for long-term or quarantine-type applications.
- If $\nu > 1$ then associated stable and unstable invariant manifolds can be determined. These orbits allow for transfers shadowing invariant manifolds to and from the orbit. Low-energy transfers are possible between two unstable orbits and may be located by analyzing Poincaré maps in the CR3BP.

### 2.3 Finding Periodic Orbits in the CR3BP

Simple co-linear periodic orbits are symmetric about the y=0 plane and intersect twice per orbit. Their intersection is orthogonal to the x-z plane (x and z axis velocity components are zero). The states of a periodic symmetric orbit are defined as $\mathbf{X}(t_0)$ and $\mathbf{X}(t_{T/2})$ where $t_0$ occurs at the first plane crossing and $t_{T/2}$ is one half a period later at the next crossing. To ensure symmetry, the initial and final states are represented as

$$\mathbf{X}(t_0) = \begin{bmatrix} x_0 & 0 & z_0 & 0 & \dot{y}_0 & 0 \end{bmatrix}^T \tag{7}$$

$$\mathbf{X}(t_{T/2}) = \begin{bmatrix} x_{T/2} & 0 & z_{T/2} & 0 & \dot{y}_{T/2} & 0 \end{bmatrix}^T \tag{8}$$

An orbit is considered "periodic" if $|\dot{x}_{T/2}| < \varepsilon$ and $|\dot{z}_{T/2}| < \varepsilon$ where $\varepsilon \approx 10^{-8}$ [6]. A differential corrector, given a rough approximation of the initial state, $\mathbf{X}_0(t_0)$, and orbital period, $T_0$, is given by

$$\mathbf{X}_{n+1}(t_0) = \mathbf{X}_n(t_0) - \delta\mathbf{X}(t_0) \tag{9}$$

$$T_{n+1} = T_n - 2\delta(T/2), \tag{10}$$

where the linearized system of equations relating the final and initial states [8] are

$$\delta\mathbf{X}(t_{T/2}) \approx \Phi(t_{T/2}, t_0)\delta\mathbf{X}(t_0) + \frac{\partial \mathbf{X}}{\partial t}\delta(T/2), \tag{11}$$

$\delta\mathbf{X}(t_{T/2})$ is the deviation of the final state due to a deviation in the initial state $\delta\mathbf{X}(t_0)$, and a corresponding deviation in the orbital period $\delta(T/2)$. The time-derivative of the state $\frac{\partial \mathbf{X}}{\partial t}$ is computed at the second plane crossing. The initial state must have an orthogonal crossing with the x-z plane thus $\dot{x} = \dot{z} = 0$, the initial and final state deviations are then

$$\begin{aligned} \delta\mathbf{X}(t_0) &= \begin{bmatrix} \delta x_0 & 0 & \delta z_0 & 0 & \delta\dot{y}_0 & 0 \end{bmatrix}^T \\ \delta\mathbf{X}(t_{T/2}) &= \begin{bmatrix} \delta x_{T/2} & -y_{T/2} & \delta z_{T/2} & -\dot{x}_{T/2} & \delta\dot{y}_{T/2} & -\dot{z}_{T/2} \end{bmatrix}^T \end{aligned}$$

Equation 11 then simplifies to

$$\begin{bmatrix} \delta x_{T/2} \\ -y_{T/2} \\ \delta z_{T/2} \\ -\dot{x}_{T/2} \\ \delta\dot{y}_{T/2} \\ -\dot{z}_{T/2} \end{bmatrix} \approx \begin{bmatrix} \phi_{11} & \phi_{12} & \phi_{13} & \phi_{14} & \phi_{15} & \phi_{16} \\ \phi_{21} & \phi_{22} & \phi_{23} & \phi_{24} & \phi_{25} & \phi_{26} \\ \phi_{31} & \phi_{32} & \phi_{33} & \phi_{34} & \phi_{35} & \phi_{36} \\ \phi_{41} & \phi_{42} & \phi_{43} & \phi_{44} & \phi_{45} & \phi_{46} \\ \phi_{51} & \phi_{52} & \phi_{53} & \phi_{54} & \phi_{55} & \phi_{56} \\ \phi_{61} & \phi_{62} & \phi_{63} & \phi_{64} & \phi_{65} & \phi_{66} \end{bmatrix}_{(t_{T/2}, t_0)} \begin{bmatrix} \delta x_0 \\ 0 \\ \delta z_0 \\ 0 \\ \delta\dot{y}_0 \\ 0 \end{bmatrix} + \begin{bmatrix} \dot{x}_{T/2} \\ \dot{y}_{T/2} \\ \dot{z}_{T/2} \\ \ddot{x}_{T/2} \\ \ddot{y}_{T/2} \\ \ddot{z}_{T/2} \end{bmatrix} \delta(T/2) \tag{12}$$

Three equations from the second, fourth, and sixth rows of equation 12 are used to solve for three unknowns via

$$\begin{aligned} -y_{T/2} &= \phi_{21}\delta x_0 + \phi_{23}\delta z_0 + \phi_{25}\delta\dot{y}_0 + \dot{y}_{T/2}\delta(T/2) \\ -\dot{x}_{T/2} &= \phi_{41}\delta x_0 + \phi_{43}\delta z_0 + \phi_{45}\delta\dot{y}_0 + \ddot{x}_{T/2}\delta(T/2) \\ -\dot{z}_{T/2} &= \phi_{61}\delta x_0 + \phi_{63}\delta z_0 + \phi_{65}\delta\dot{y}_0 + \ddot{z}_{T/2}\delta(T/2), \end{aligned}$$

**Case One:** If the orbital period, $T$, is fixed such that $\delta(T/2) = 0$, then $x_0$, $z_0$, and $\dot{y}_0$ are free,

$$\begin{bmatrix} \delta x_0 \\ \delta z_0 \\ \delta\dot{y}_0 \end{bmatrix} = \begin{bmatrix} \phi_{21} & \phi_{23} & \phi_{25} \\ \phi_{41} & \phi_{43} & \phi_{45} \\ \phi_{61} & \phi_{63} & \phi_{65} \end{bmatrix}^{-1} \begin{bmatrix} y_{T/2} \\ \dot{x}_{T/2} \\ \dot{z}_{T/2} \end{bmatrix}.$$

**Case Two:** If $x_0$ is fixed such that $\delta x_0 = 0$, then $z_0$, $\dot{y}_0$, and $T$ are free,

$$\begin{bmatrix} \delta z_0 \\ \delta\dot{y}_0 \\ \delta(T/2) \end{bmatrix} = \begin{bmatrix} \phi_{23} & \phi_{25} & \dot{y}_{T/2} \\ \phi_{43} & \phi_{45} & \ddot{x}_{T/2} \\ \phi_{63} & \phi_{65} & \ddot{z}_{T/2} \end{bmatrix}^{-1} \begin{bmatrix} y_{T/2} \\ \dot{x}_{T/2} \\ \dot{z}_{T/2} \end{bmatrix}.$$

**Case Three:** If $z_0$ is fixed such that $\delta z_0 = 0$, then $x_0$, $\dot{y}_0$, and $T$ are free,

$$\begin{bmatrix} \delta x_0 \\ \delta \dot{y}_0 \\ \delta(T/2) \end{bmatrix} = \begin{bmatrix} \phi_{21} & \phi_{25} & \dot{y}_{T/2} \\ \phi_{41} & \phi_{45} & \ddot{x}_{T/2} \\ \phi_{61} & \phi_{65} & \ddot{z}_{T/2} \end{bmatrix}^{-1} \begin{bmatrix} y_{T/2} \\ \dot{x}_{T/2} \\ \dot{z}_{T/2} \end{bmatrix}.$$

**Case Four:** If $\dot{y}_0$ is fixed such that $\delta \dot{y}_0 = 0$, then $x_0$, $z_0$, and $T$ are free,

$$\begin{bmatrix} \delta x_0 \\ \delta z_0 \\ \delta(T/2) \end{bmatrix} = \begin{bmatrix} \phi_{21} & \phi_{23} & \dot{y}_{T/2} \\ \phi_{41} & \phi_{43} & \ddot{x}_{T/2} \\ \phi_{61} & \phi_{63} & \ddot{z}_{T/2} \end{bmatrix}^{-1} \begin{bmatrix} y_{T/2} \\ \dot{x}_{T/2} \\ \dot{z}_{T/2} \end{bmatrix}.$$

### 2.4 Transitioning from CR3BP to an N-body Ephemeris Model

The NASA General Mission Analysis Tool (GMAT) was used to model the higher-fidelity planetary ephemeris and verify these CR3BP orbits maintained their quasi-periodic properties [9]. The Planetary and Lunar Ephemeris DE 421 model was invoked through GMAT to precisely determine the position and velocity of the moon [10]. The ephemeris transition process from the CR3B model to the high fidelity GMAT force model, consisted of 66 or more patch points per orbital period and then correcting them via multi-level shooting technique. The multi-level shooting technique employs a two-level differential correction process [11]:

- Level One - differential correction process operates on the velocity components of each patch point. The resulting output is a continuous ballistic trajectory in the higher fidelity force model (no discontinuities in position after a single pass). This process is embarrassingly parallel as the corrector can operate on each segment separately. The velocity components at the start of each segment can be corrected simultaneously
- Level Two - differential correction process operates on the position and epoch of all patch points concurrently. The resulting output is a smooth trajectory which has minimal discontinuities in velocities between segments. This process operates on all segments at once using a minimum-norm solution of least-square system to drive discontinuities in velocity (delta-v) down to zero.

A smooth continuous trajectory was obtained after several iterations of the multi-level shooting method. This smoothed trajectory was propagated for several orbital periods using a numerical ordinary differential equation solver on the higher-fidelity force model. The resulting properties of each trajectory were compared against those of the CR3B orbit to verify their periodicity and stability was maintained.

## 3. CONSTRUCTION OF TULIP-SHAPED ORBITS

The focus of this research is on the Earth-Moon system, therefore averaged constants, obtained from the JPL three-body periodic orbit database, are used for dimensionalization and displayed in Table 1.

| Parameter | Symbol | Value | Units |
|---|---|---|---|
| Mass Ratio | $\mu$ | $1.215058560962404 \times 10^{-2}$ | |
| Length Unit (LU) | $l*$ | 389703 | km |
| Time Unit (TU) | $t*$ | 382981 | s |

Table 1: Parameters obtained from the JPL three-body periodic orbit database.

A dimensionless state vector and corresponding period, found by constructing a third order analytic halo orbit about the second Earth-Moon Lagrange Point, is provided in Table 2 [12]. The process of iterating equations 9-10, while holding the $x_0$ coordinate fixed, provided a solution for the remaining free variables ($z_0$, $\dot{y}_0$, $\tau_0$). Several thousand iterations consisting of fixed step size increments on the order of $\delta x = 10^{-4}$ were run until NRHOs were generated with perilune altitudes near zero.

| x | y | z | $\dot{x}$ | $\dot{y}$ | $\dot{z}$ | $\tau_0$ |
|---|---|---|---|---|---|---|
| 1.11808849729283 | 0.0 | -0.0223152933461533 | 0.0 | 0.185335512941906 | 0.0 | 3.40271361070999 |

Table 2: Halo Orbit Constructed by a Third Order Analytic Solution ($A_z = 10$ Mm) About $L_2$

Figure 1 depicts the family of halo orbits generated from the initial state in Table 2. Notice as the orbits approach the Moon, the y-axis amplitude gets smaller and they become NRHOs.

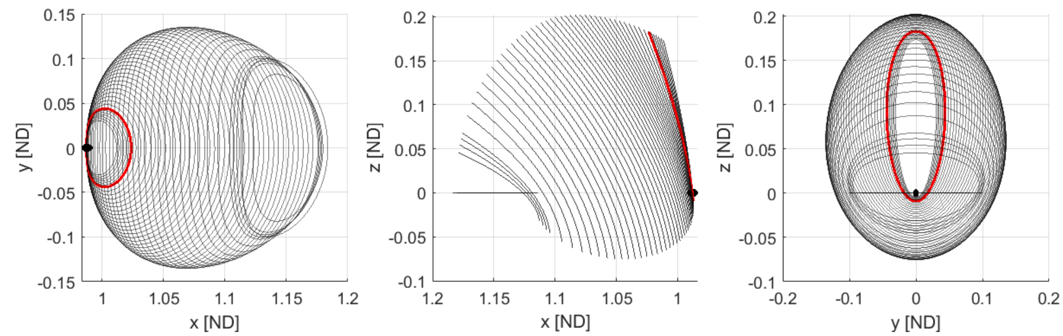


Fig. 1: Halo Orbit Family About $L_2$ (Red = 1,830 km Perilune Altitude NRHO)

Initial states, orbital periods, stability indices, perilune and apolune altitudes associated with this family are provided in Table 3. Note, as the initial states are co-linear with the Earth-Moon vector, the $y$, $\dot{x}$, and $\dot{z}$ components are all zero.

| x | z | $\dot{y}$ | $\tau_0$ | $\nu$ | $\mathbf{r_{min}}$ [km] | $\mathbf{r_{max}}$ [km] |
|---|---|---|---|---|---|---|
| 1.013531 | 0.175476 | -0.083989 | 1.397814 | 1.059799 | 336.389366 | 67,374.787632 |
| **1.023731** | **0.183250** | **-0.106950** | **1.533637** | **1.369020** | **1,829.784441** | **71,031.977339** |
| 1.042531 | 0.193367 | -0.143803 | 1.787043 | 1.686317 | 5,406.145598 | 76,573.641934 |
| 1.062131 | 0.200020 | -0.175270 | 2.069754 | 1.356538 | 10,092.511198 | 81,413.009476 |
| 1.081731 | 0.202351 | -0.199740 | 2.365015 | 1.000000 | 15,557.344385 | 85,193.428640 |
| 1.101131 | 0.198617 | -0.216510 | 2.650791 | 6.543638 | 21,527.179400 | 87,369.121704 |
| 1.120731 | 0.186215 | -0.224868 | 2.906681 | 22.413172 | 27,839.528342 | 87,413.242899 |
| 1.140331 | 0.162882 | -0.223312 | 3.111210 | 64.993762 | 34,187.749702 | 85,212.270523 |
| 1.159931 | 0.124889 | -0.208757 | 3.268499 | 179.779216 | 40,677.690364 | 81,123.512274 |
| 1.179531 | 0.036552 | -0.163145 | 3.404549 | 547.882115 | 48,997.107897 | 74,307.806621 |

Table 3: Dimensionless Halo Orbit States, Period, Stability, and Min/Max Altitudes

An interesting discovery occurred during this research where the initial state of an NRHO with a perilune altitude of 1,830 km ($r_p \approx 3,568$ km) would fork into other periodic orbits after changing the orbital period of a new orbit and fixing the x-axis (equation 12, case two). Entire families of periodic orbits were found with their unique properties documented in section 3.1. The initial states for the tulip-shaped orbit family occurs along the x-axis at a location near $x_0 = 1.023731$. Table 4 depicts the forked dimensionless states, their corresponding period, stability index, and perilune/apolune altitudes of tulip-shaped orbits with petal counts up to 15. Note that these states correspond to the same x-axis location which may result in perilune altitudes that are below the lunar surface. The same iterative procedure to generate the family of halo orbits, equations 9-10, can be applied to increment the x-axis and resolve for the reaming free variables ($z_0$, $\dot{y}_0$, and $\tau_0$).

| $\mathbf{N_p}$ | $\mathbf{x}$ | $\mathbf{z}$ | $\dot{\mathbf{y}}$ | $\boldsymbol{\tau_0}$ | $\nu$ | $\mathbf{r_{min}}$ [km] | $\mathbf{r_{max}}$ [km] |
|---|---|---|---|---|---|---|---|
| 1 | 1.023731 | 0.183250 | -0.106950 | 1.533637 | 1.369020 | 1,829.784441 | 71,031.977339 |
| 2 | ↓ | 0.174305 | -0.082095 | 2.756426 | 1.143759 | 252.101807 | 67,614.276846 |
| 3 | | 0.159022 | -0.049901 | 3.588824 | 1.000000 | -752.494538 | 61,792.204570 |
| 4 | | 0.138427 | -0.016770 | 4.050042 | 1.006718 | -985.883719 | 53,991.239415 |
| 5 | | 0.122012 | 0.006413 | 4.380388 | 1.000000 | -868.057171 | 47,824.858055 |
| 6 | | 0.108984 | 0.026199 | 4.628880 | 1.000070 | -652.016695 | 42,976.890137 |
| 7 | | 0.098423 | 0.044549 | 4.827278 | 1.000000 | -399.673136 | 39,087.918798 |
| 8 | | 0.089585 | 0.062522 | 4.991642 | 1.000000 | -125.782171 | 35,870.635633 |
| 9 | | 0.081981 | 0.080721 | 5.131974 | 1.000000 | 167.602678 | 33,137.365975 |
| 10 | | 0.075272 | 0.099631 | 5.254942 | 1.000000 | 485.029409 | 30,759.162050 |
| 11 | | 0.069206 | 0.119765 | 5.365409 | 1.000000 | 836.201072 | 28,641.991429 |
| 12 | | 0.063570 | 0.141824 | 5.467385 | 1.000000 | 1,238.547091 | 26,710.271479 |
| 13 | | 0.058150 | 0.167010 | 5.564950 | 1.000000 | 1,724.825262 | 24,891.061674 |
| 14 | | 0.052617 | 0.198057 | 5.664248 | 1.000000 | 2,376.009532 | 23,082.050586 |
| 15 | | 0.045796 | 0.247118 | 5.787296 | 1.000000 | 3,566.416573 | 20,935.315380 |

Table 4: Dimensionless Earth-Moon Tulip-Shaped States, Period, Stability, and Min/Max Altitudes

Figure 2 displays a curve fit of the three free variables, $z$, $\dot{y}$, and $\tau$, needed to form the full six dimensional state vector as well as its dimensionless orbital period as a function of the number of tulip petals. A visual depiction of each newly discovered tulip family is provided in appendix A.

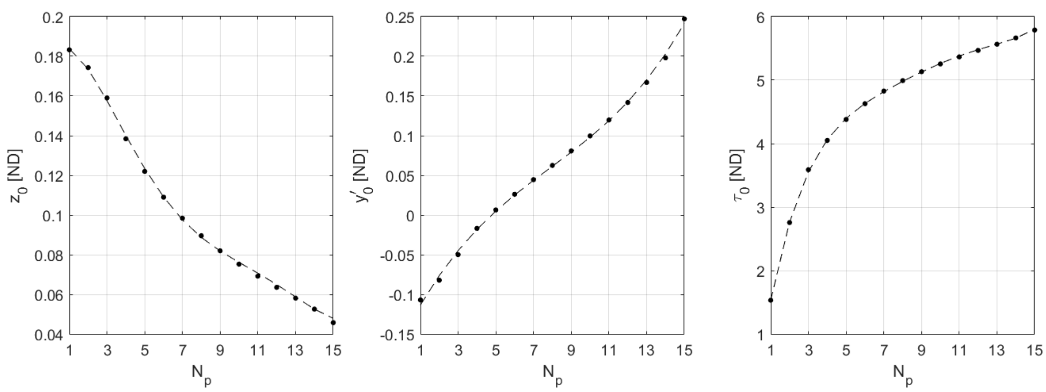


Fig. 2: Initial States of Tulip-shaped Orbits Corresponding to Number of Petals, $N_p$, (dotted line = polynomial fit)

These initial states are reduced to just three polynomial equations via,

$$
\begin{aligned}
z_0(N_p) &= 1.91 \times 10^{-6} N_p^5 - 8.55 \times 10^{-5} N_p^4 + 1.38 \times 10^{-3} N_p^3 - 9.10 \times 10^{-3} N_p^2 + 8.49 \times 10^{-3} N_p + 0.18 && (13)\\
\dot{y}_0(N_p) &= 1.59 \times 10^{-4} N_p^3 - 3.758 \times 10^{-3} N_p^2 + 4.72 \times 10^{-2} N_p - 0.16 && (14)\\
\tau_0(N_p) &= 5.02 \times 10^{-5} N_p^5 - 2.426 \times 10^{-3} N_p^4 + 4.61 \times 10^{-2} N_p^3 - 0.44 N_p^2 + 2.257 N_p - 0.33, && (15)
\end{aligned}
$$

where $N_p = [1, 2, ..., 15]$. The dimensionless initial state of a tulip-shaped orbit with $N_p$ petals can then be determined as

$$\mathbf{X}_0(N_p) \quad = \quad \begin{bmatrix} 1.023731 & 0.00 & z_0(N_p) & 0.00 & \dot{y}_0(N_p) & 0.00 \end{bmatrix},$$

where $z_0(N_p)$, $\dot{y}_0(N_p)$, and corresponding period, $\tau_0(N_p)$ are computed from equations 13-15 respectively.

The relationship between the three free variables, $z_0$, $\dot{y}_0$, and $\tau_0$, is both smooth and continuous, as shown in Figure 2. It's feasible that these polynomial curves can be extrapolated to approximate the initial state for higher petal count tulip-shaped orbits (e.g. $N_p > 15$). It would be highly informative check the consistency of this solution when determining existence in different three-body systems (e.g. using a different mass ratio, $\mu$), and if the relative slopes are maintained.

### 3.1 Families of Tulip-Shaped Orbits

Previous literature, looking for a staging location to the lunar surface, has established that two-lobe butterfly orbits, $N_p = 2$, can be found from bifurcating a $L_2$ NRHO with a perilune radius of $r_p \approx 1,830$ km [13]. In this research, it was discovered that this NRHO can be repeatedly forked into co-linear tulip-shaped orbits with up to $N_p = 15$ petals (or lobes). Figure 3 depicts all families of the newly discovered tulip-shaped orbits using a minimum perilune altitude of 500 km. Note that while a common perilune altitude was selected for these orbits, all contain families contain solutions which range from meters to mega-meters.

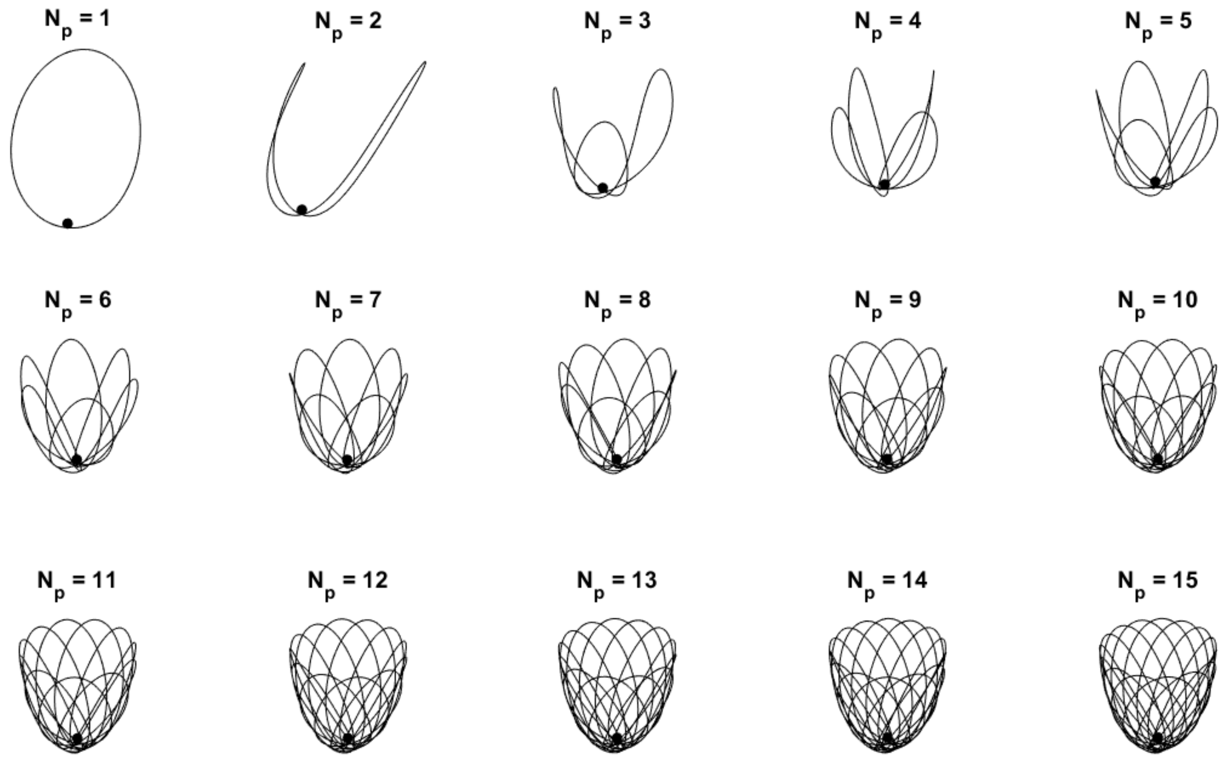


Fig. 3: Tulip-Shaped Orbits Consisting of $N_p$ Petals at 500 km Perilune Altitude (black dot = Moon)

Observations of these tulip-shaped quasi-periodic orbits are provided below:

- $\mathbf{N_p = 1}$**, NRHO** - a single lobe orbit found from a halo orbit about the Earth-Moon $L_2$. Perilune altitudes range from the lunar surface up to 50 Mm while apolune altitudes are between 60 -90 Mm. The stability index is above 1 for many altitudes suggesting that stable and unstable manifolds exist. The Jacobi constant for these orbits are the lowest of all forked orbits with dimsionless periods ranging anywhere from one fourth to one half a lunar orbital period.
- $\mathbf{N_p = 2}$**, Butterfly Orbit** - a bifurcated NRHO with perilune altitudes ranging between the lunar surface upto 15 Mm. Apolune altitudes range between 60-70Mm. The stability index is higher than that of the NRHO and above unity suggesting there are more stable and unstable transfer manifolds into this orbit. The Jacobi constant is slightly higher than that of an NRHO allowing for direct transfers between the two families. The orbital period is about 1.8 times that of an NRHO. This orbit was previously discovered and published by Whitley et al [13] in his analysis of orbits for lunar surface exploration.

- $\mathbf{N_p = 3}$, **Three-Petal Tulip-shaped Orbit** - a trifurcated NRHO with a stability index near unity until perilune altitudes exceed 3.5 Mm.
- $\mathbf{N_p = 4}$, **Four-Petal Tulip-shaped Orbit** - a quadfurcation NRHO with a stability index above unity for all perilune altitudes. This is the last orbit in the family to have a stability index above unity.
- $\mathbf{N_p = 5-15}$, **Multi-Petal Tulip-shaped Orbits** - a forked NRHO orbit into multiple petals, all with stability indicies near unity. These orbits may be good candidates for SDA survellance applications as they have low stationkeeping requirements. The apolune altitude decreases with each additional petal, from 48 Mm to 20 Mm. Note that the $N_p = 6$ tulip-shaped orbit has been published in previous studies as it was independently discovered through the use of 2D Poincaré maps [5].

Figure 4 shows that higher petal count tulip-shaped orbits have lunar inclinations that converge near 63 degrees as $N_p$ is increased. After the three-petal tulip-orbit, contains inclinations between 65 and 80 degrees at perilune and apolune respectively, the spread decreases to less than two degrees by fifteen petals. It appears that these higher petal count orbits may converge into a specific Lunar Frozen Orbit (LFO) configuration [14]. LFOs have a similar inclination spread relative to the Earth-Moon orbit plane frame of reference while their eccentricity and semi-major axis remain relatively fixed. The range of inclinations for each tulip-shaped orbit also exists within the bounds of critical inclination for the Earth-Moon system, $i \in [39.2°, 140.77°]$.

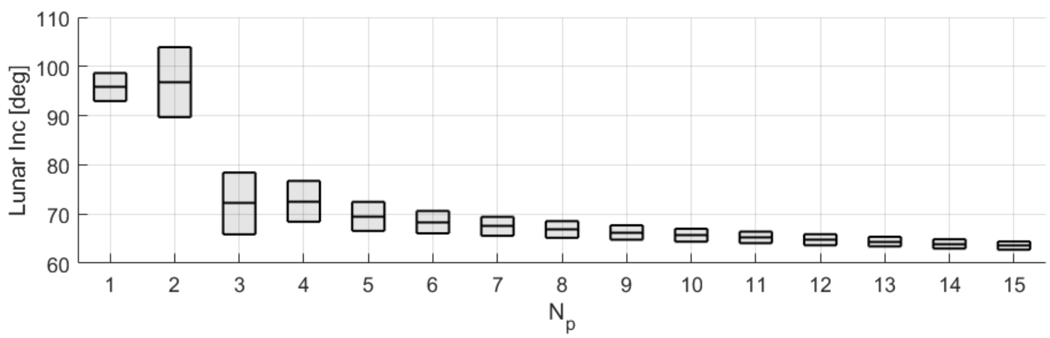


Fig. 4: Lunar Inclination vs $N_p$ Petals at 500 km Perilune Altitude

Figure 5 shows that the apolune altitudes for each tulip-shaped orbit family decreases with an increase in petal count (for a fixed perilune altitude of 500 km). Comparatively, an LFO with a 500 km perilune altitude at an inclination of 63.58° and eccentricity of $\sqrt{0.17 - 0.83\cos 2i} = 0.82$ has an apolune altitude near 20,690 km. For reference, the lowest apolune altitude of the tulip-shaped orbit families occurs at $N_p = 15$ and is nearly 2,700 km higher.

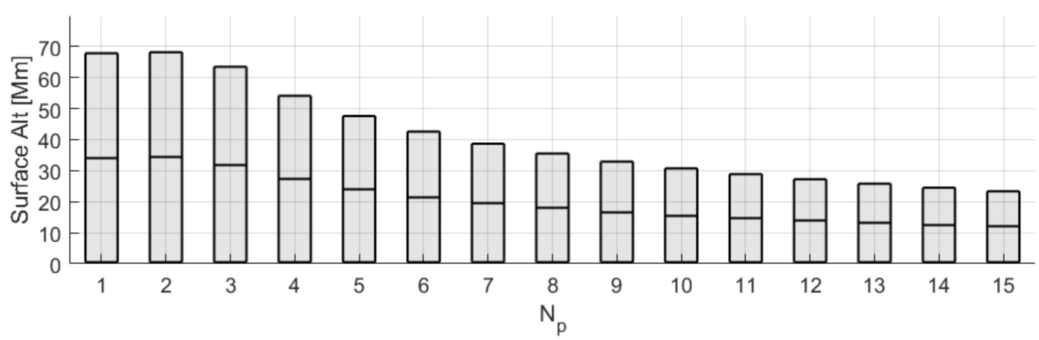


Fig. 5: Lunar Altitude vs $N_p$ Petals at 500 km Perilune Altitude

Borrowing the concept used for bifurcation analysis, a family of periodic solutions is a set of solutions sharing a common hodograph [15]. In the context of three-body dynamics, a hodograph is a continuous curve in phase space that consists of points belonging to different periodic solutions [16]. Specifically, this phase space contains six dimensions, however symmetric periodic solutions contain at least two mirror configurations, furthermore, initial conditions dictate states of three non-zero parameters. It's possible to move along the hodograph by varying a system parameter such as Jacobi's constant such that periodic solutions continuously evolve. A point along the hodograph at which the stability changes is referred to as a bifurcation point. Figures 6 and 7 respectively depict a hodographs of the Jacobi constant and stability index as a function of perilune altitude.

Note that a hodograph bifurcation point occurs between the NRHO and Butterfly orbit near 100 km in perilune altitude ($r_p \approx 1,830$ km). The $N_p = 3$ to $N_p = 13$ petal count tulip-shaped orbits do not bifurcate at perilune altitudes below 5 Mm until higher petal counts of $N_p = 14$ are reached. There is another bifrucation identified between 14 and 15 petal tulip orbits near a perilune altitude of 2,600 km ($r_p \approx 4,338$ km) The stability index hodograph indicates possible low-energy transfer manifolds for all tulip orbits with a petal count below $N_p = 5$. Looking at the Jacobi constant, there are clearly defined separations, $\Delta J$, for each additional petal which are maintained throughout all perliune altitudes.

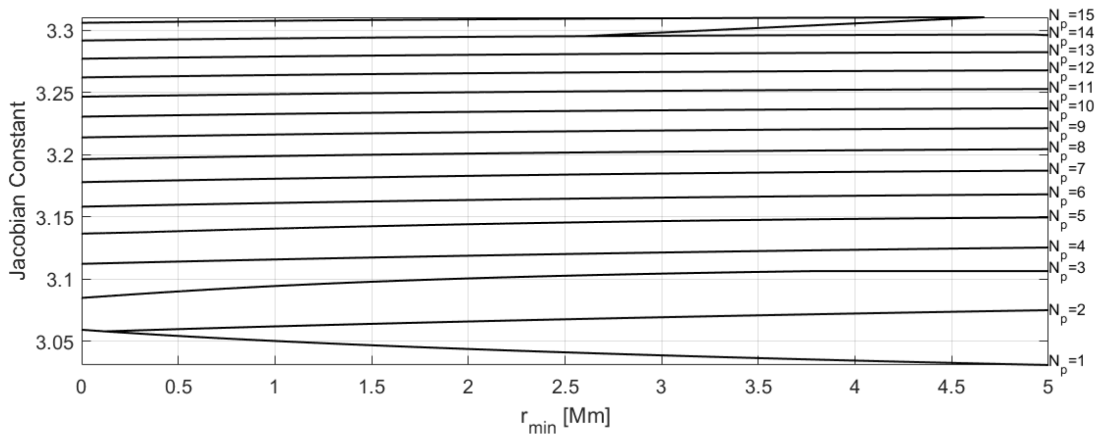


Fig. 6: Jacobi Constant vs Perilune Alt Hodograph of Tulip-Shaped Orbits With Petals $N_p \in [1, 15]$.

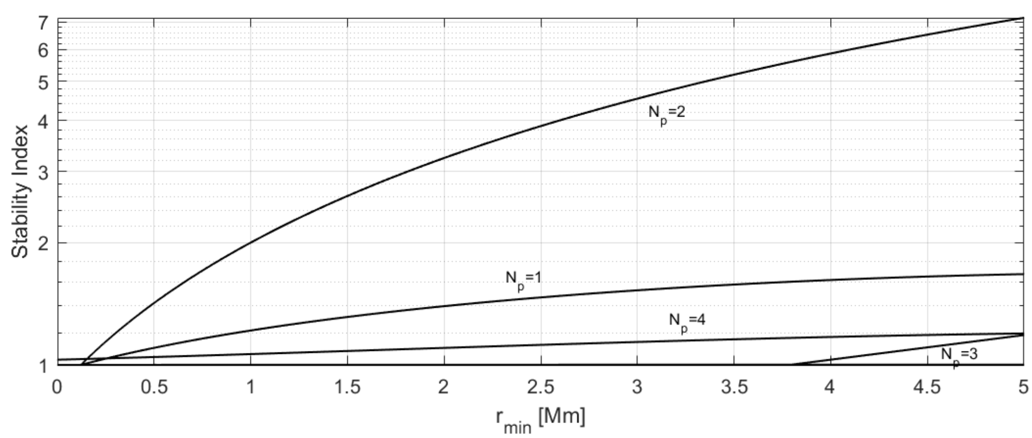


Fig. 7: Stability Index vs Perilune Alt Hodograph of Tulip-Shaped Orbits With Petals $N_p \in [1, 15]$.

A spacecraft that has a Jacobi constant value under 2.988 can theoretically reach any point within the Earth-Moon system. Higher Jacobi constants signify that access to available regions of space are more restricted which, like stability indices near unity, are better for lunar quarantine and SDA type applications. The minimum number of instantaneous $\Delta V$ impulses can be determined from the Jacobi constant and the orbit stability, transfers between two stable orbits require a minimum of two $\Delta V$ impulses while transfers between unstable and stable orbits as well as two unstable orbits can be performed with a single $\Delta V$ impulse [8].

### 3.2 Higher Fidelity Ephemeris Model

Using the procedure described in 2.4, the tulip-shaped CR3BP orbits were transitioned to an N-body model using the DE 421 lunar and planetary ephemeris. The results for several tulip-shaped orbit families are displayed in figure 8. Note that the moon was included in each subplot and its diameter is properly scaled for reference.

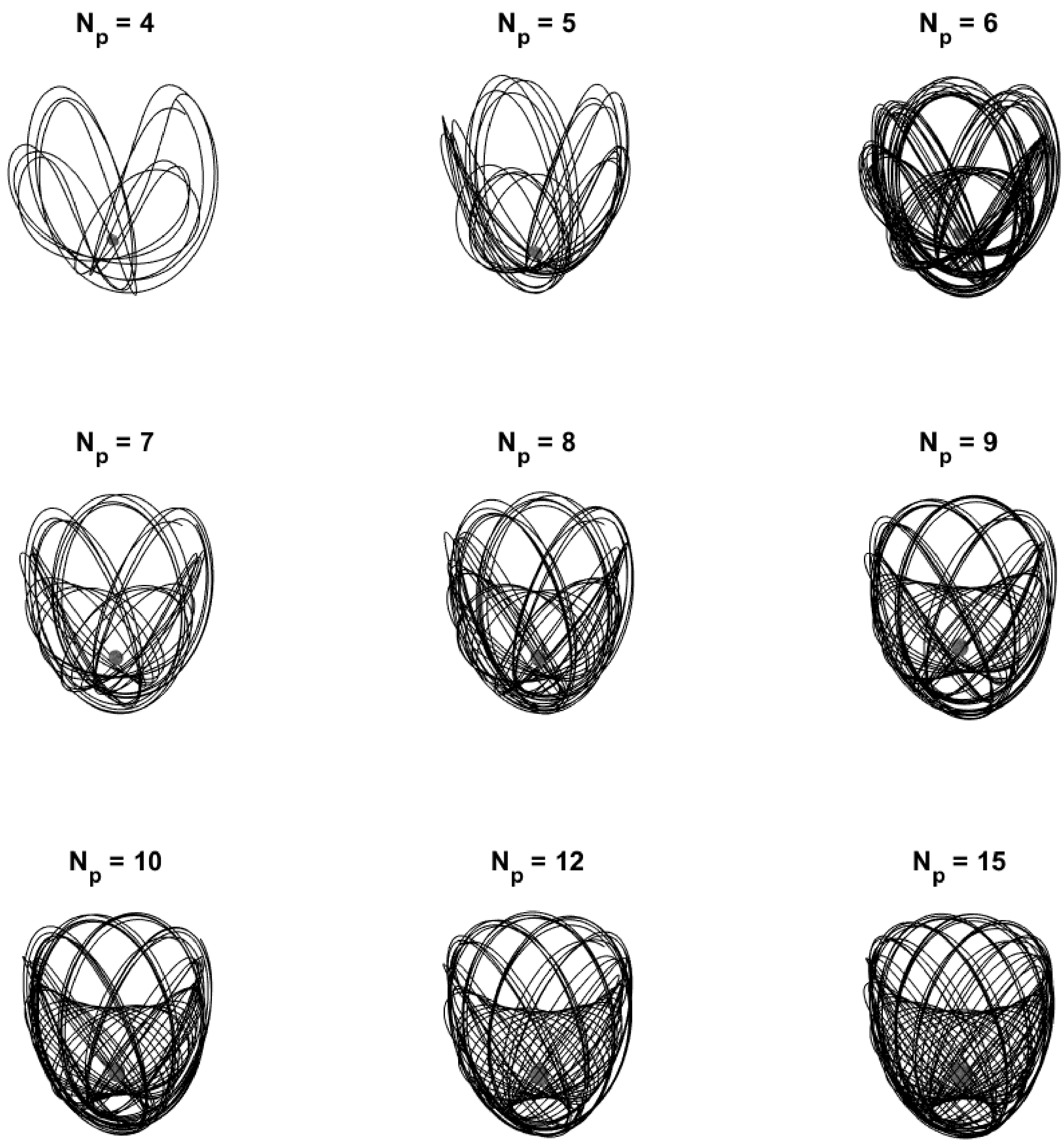


Fig. 8: Tulip-Shaped Orbits After Transitioning from the CR3BP to the DE 421 Lunar Ephemeris

Each example consisted of between 3-15 periods (62 to 275 days). Depending on the number of petals in the periodic orbit, between 55 and 100 patch points were used in the multi-level shooting method. After $N_p = 4$, it became significantly easier to find the correct combination of patch points and perilune altitude that quickly converged, this appears related to the stability properties of the orbit and the location of each patch point. From a preliminary literature review, it appears that these findings translate to other three-body systems as well. As noted in section 3.1, the $N_p = 6$ tulip-shaped orbit was discovered and published in a previous study using a 2D Poincaré map on Titan, Saturn's largest moon [5].

# 4. ASSUMPTIONS

## 4.1 Target Catalog and Coverage Metrics

Fifteen cislunar trajectories, consisting of eight orbit families, were selected about the Earth-Moon system. Their corresponding state vectors are provided in a previous study evaluating the orbit determination benefits of moon-based sensors [17]. The final NASA catalog of manmade material on the Moon, with several slight corrections, was used to establish the Selenographic coordinates of 64 individual target locations [18]. Figure 9 depects all cislunar target trajectories as well as the surface targets used for this study.

A subset of coverage metrics described in a previous study on hosted payload architectures for improved GEO SSA [19] were modified for use in cislunar architectures and briefly described below

- **Total Number of Tracks** - Total number of tracking intervals over the analysis period. Indicates the number of times favorable viewing conditions exist.
- **Total Track Duration** - Sum of each track duration. This indicates an orbit's near-continuous coverage performance.
- **Average max tracking gap** - Time from the end of one track to the beginning of the next track for each catalog object, the maximum gap over the analysis period is computed, then averaged across the population. This indicates worst-case revisit times for a given orbit.
- **Average min tracking gap** Similar to the average max tracking gap, but minimum is computed instead. This indicates the best-case revisit times for a given orbit.

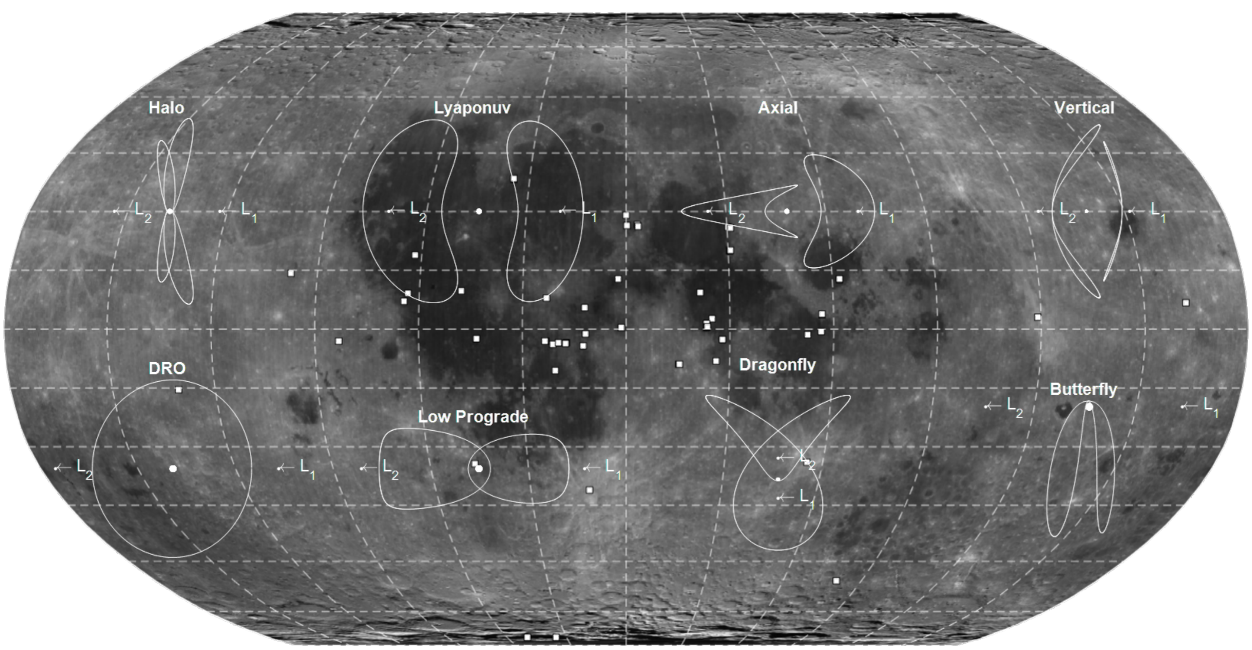


Fig. 9: 15 Target Trajectories (lines) and 64 Surface Targets from NASA's Man-made Material on the Moon (squares).

## 5. RESULTS AND DISCUSSION

A thousand trial Monte Carlo simulation was performed over a full Earth year with 15 minute time steps and randomly varied starting locations of all three-body trajectories. Coverage metrics were computed for each target and averaged across all trials. As this study was intended to be agnostic to sensor phenomenology, solar exclusions and minimum elevation angles were not considered. A track was counted when the line of sight between the sensor and the target was unobstructed by the moon. All orbit configurations, except for the NRHO, provided full coverage of all targets within the catalog. The gap time and track duration performance for each tulip-shaped orbit is presented in Figure 10.

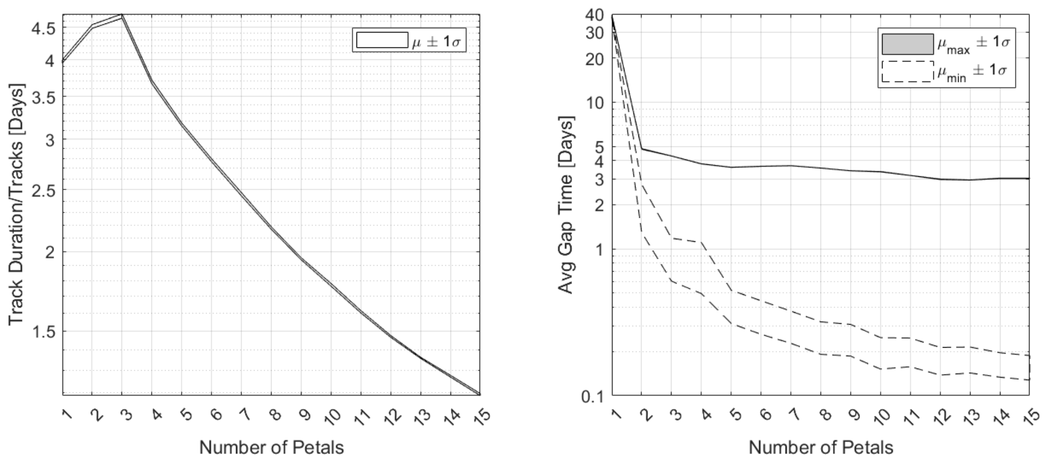


Fig. 10: Total Track Duration/ Number of Tracks (left) and Average Min/Max Gap Times (right)

Notice that as higher petal count orbits are considered, the average maximum and minimum gap times of tracking both lunar-based and space-based targets decrease. Higher petal count tulip-shaped orbits offer better gap time performance while tulip-shaped orbits closer to 3 petals offer longer overall duration tracks for persistent monitoring. NRHO orbits cannot maintain coverage of all cataloged objects as they do not offer 360 degree LOS viewing of the lunar surface. While it is clear that higher petal counts reduce both the maximum and minimum average gap times across all cataloged objects, there is an exponential decrease in gap times for the minimum case and gradual linear decrease for the maximum case. These results only depict the performance of a single satellite in each orbit configuration, gap times will decrease proportional to their number and spacing.

## 6. CONCLUSIONS AND FUTURE WORK

Entirely new families of three-body quasi periodic trajectories, termed "tulip-shaped orbits" were discovered and presented for the first time in scientific literature. A subset of these families have a stability index above unity suggesting the existence of low-energy transfers between other orbits. All tulip-shaped orbits were successfully transitioned to a high precision lunar ephemeris model using a well established multi-level shooting technique. Three polynomial equations were developed, as a function of petal count, to obtain the initial states of each tulip-shaped orbit family. A differential corrector can then be used to converge upon the desired periodic orbit and its desired period along with perilune and apolune altitudes can be adjusted via iterative process. All new families of orbits were evaluated for their gap time and track duration coverage against the NASA man-made catalog of material on the lunar surface and fifteen previously published cislunar trajectories. Findings demonstrate that average minimum and maximum gap times decrease with an increase in petals.

Additional areas of research that warrant further investigation as a result of the above findings include:

- Station Keeping and Orbital Maintenance - after existence has been established in a high precision lunar ephemeris model, an orbital maintenance technique can be developed to maintain the trajectory for an extended time period. Assessing how to maintain spacing between several space vehicles would be beneficial for constellation formation and maintenance.

- Low-Energy Transfers - inserting a spacecraft via manifold may be possible for those with stability indicies above unity. Further identifying techniques to assist mission designers in performing impulsive and low-thrust orbit transfer between orbit families would add utility.
- Communications and Navigation - families of these orbits have several desirable properties for lunar surface navigation and communication systems as their apolune altitudes decrease down to 20 Mm with an increase in petal count. Orbits are stationary with respect to the Earth-Moon rotating frame placing perilune and apolune over the same selenographic coordinates (e.g. repeating ground tracks). Many families are neutrally stable suggesting low station-keeping and end-of-life $\Delta V$ requirements.
- Additional Periodic Families - while the tulip-shaped orbits discussed are three-dimensional, similar planar periodic trajectories were also observed in the CR3BP. There may be additional orbits with a higher petal counts offering lower apolune altitudes and greater geometric variety. There may be a similar family or orbits that can be forked from an $L_1$ NRHO.
- Checking Additional Three-Body Systems - this research was focused on the Earth-Moon system, as pointed out during the discover that the initial states are both smooth and continuous with respect to the petal count, does this change when a different mass ratio is used?
- Constellation Design - tulip-shaped orbits may offer better overall SDA performance benefits when combined with more traditional two-body or other halo type orbits. This may need to be assessed by looking at various metrics in a complete sensor architecture.

In addition to the above areas of research, further extending bifurcation theory to analytically reproduce these new orbit families in other three-body systems (e.g. Sun-Earth, Saturn-Titan) would benefit many deep space missions and advance our understanding of circular restricted three-body dynamics.

## 7. ACKNOWLEDGMENTS

The author would like to thank Raytheon's space systems business unit for sponsoring this research.

## 8. REFERENCES


[1] H. Poincaré, "Méthodes nouvelles de la mécanique céleste (new methods of celestial mechanics, english translation)," *Am. Inst. of Phys., Woodbury, NY*, pp. 1892–1899, 1993.

[2] F. Griffin and F. Moulton, "Periodic orbits," *Washington, Carnegie Institute of Washington Publication*, no. 161, 1920.

[3] M. Vaquero and J. Senent, "Poincaré: A multi-body, multi-system trajectory design tool," 2018.

[4] D. C. Davis, R. J. Power, K. C. Howell, and J. P. Gutkowski, "Lunar impact probability for spacecraft in near rectilinear halo orbits," in *AAS/AIAA Space Flight Mechanics Meeting, Virtual*, 2021.

[5] D. C. Davis, S. M. Phillips, and B. P. McCarthy, "Trajectory design for saturnian ocean worlds orbiters using multidimensional poincaré maps," *Acta Astronautica*, vol. 143, pp. 16–28, 2018.

[6] K. Connor Howell, "Three-dimensional, periodic,'halo'orbits," *Celestial mechanics*, vol. 32, no. 1, pp. 53–71, 1984.

[7] D. J. Grebow, M. T. Ozimek, K. C. Howell, and D. C. Folta, "Multibody orbit architectures for lunar south pole coverage," *Journal of Spacecraft and Rockets*, vol. 45, no. 2, pp. 344–358, 2008.

[8] J. S. Parker and R. L. Anderson, *Low-energy lunar trajectory design*, vol. 12. John Wiley & Sons, 2014.

[9] S. P. Hughes, "General mission analysis tool (gmat)," tech. rep., 2016.

[10] W. M. Folkner, J. G. Williams, and D. H. Boggs, "The planetary and lunar ephemeris de 421," *IPN progress report*, vol. 42, no. 178, p. 1, 2009.

[11] B. G. Marchand, K. C. Howell, and R. S. Wilson, "Improved corrections process for constrained trajectory design in the n-body problem," *Journal of Spacecraft and Rockets*, vol. 44, no. 4, pp. 884–897, 2007.

[12] D. L. Richardson, "Analytic construction of periodic orbits about the collinear points," *Celestial mechanics*, vol. 22, no. 3, pp. 241–253, 1980.

[13] R. J. Whitley, D. C. Davis, L. M. Burke, B. P. McCarthy, R. J. Power, M. L. McGuire, and K. C. Howell, "Earth-moon near rectilinear halo and butterfly orbits for lunar surface exploration," in *AAS/AIAA Astrodynamics Specialists Conference, Snowbird, Utah*, 2018.

[14] D. Folta and D. Quinn, "Lunar frozen orbits," in *AIAA/AAS Astrodynamics Specialist Conference and Exhibit*, p. 6749, 2006.

[15] C. Goudas, "Three-dimensional periodic orbits and their stability," *Icarus*, vol. 2, pp. 1–18, 1963.

[16] K. Howell and E. Campbell, "Three-dimensional periodic solutions that bifurcate from halo families in the circular restricted three-body problem (aas 99-161)," *Advances in the Astronautical Sciences*, vol. 102, pp. 891–910, 1999.

[17] D. C. Koblick and J. S. Choi, "Cislunar orbit determination benefits of moon-based sensors," 2022.

[18] NASA, "Final catalog of manmade material on the moon." `https://history.nasa.gov/FINAL%20Catalogue%20of%20Manmade%20Material%20on%20the%20Moon.pdf`, 2012. [Online; accessed 06-June-2023].

[19] D. Vallado, J. Lowe, and J. Anderson, "Benefits of hosted payload architectures for improved geo ssa," in *Advanced Maui Optical and Space Surveillance Technologies Conference*, p. E26, 2011.

## A. TULIP-SHAPED ORBIT FAMILIES STEMMING FROM AN $L_2$ NRHO

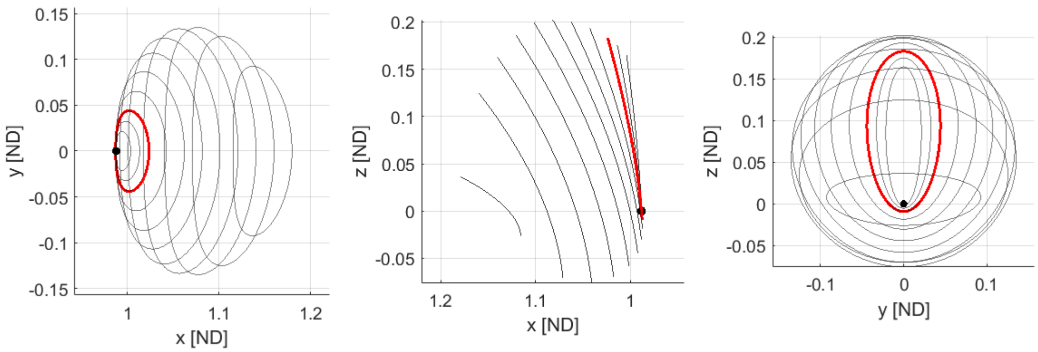


Fig. 11: $N_p = 1$ Halo Orbit Family About $L_2$ (Red = Bifurcated Solution from 1,800 km NRHO)

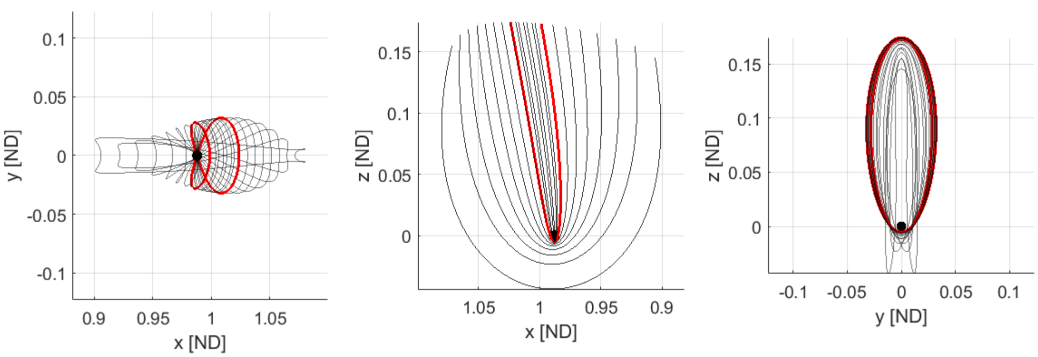


Fig. 12: $N_p = 2$ Butterfly Orbit Family About $L_2$ (Red = Bifurcated Solution from 1,800 km NRHO)

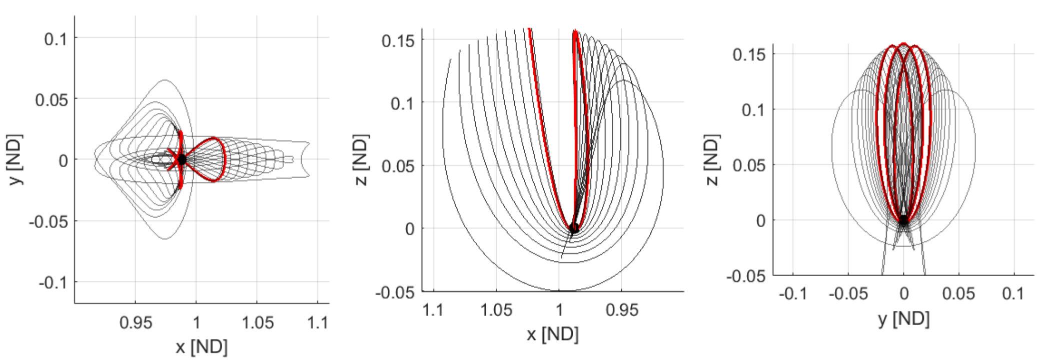


Fig. 13: $N_p = 3$ Tulip-shaped Orbit Family About $L_2$ (Red = Trifurcated Solution from 1,800 km NRHO)

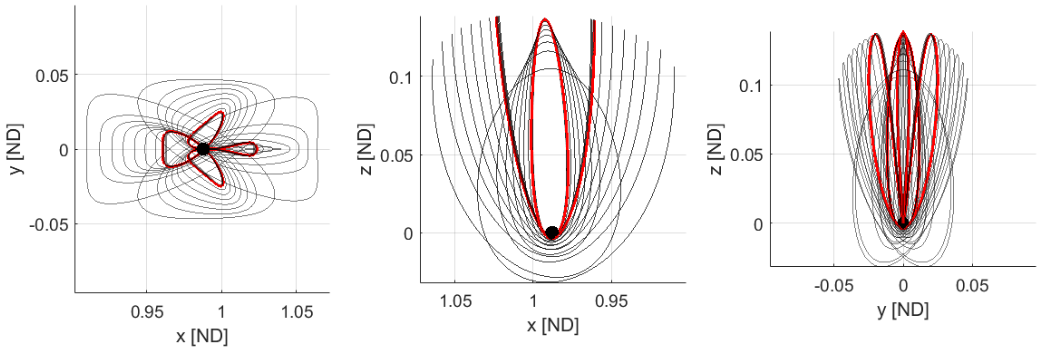


Fig. 14: $N_p = 4$ Tulip-shaped Orbit Family About $L_2$ (Red = Forked Solution from 1,800 km NRHO)

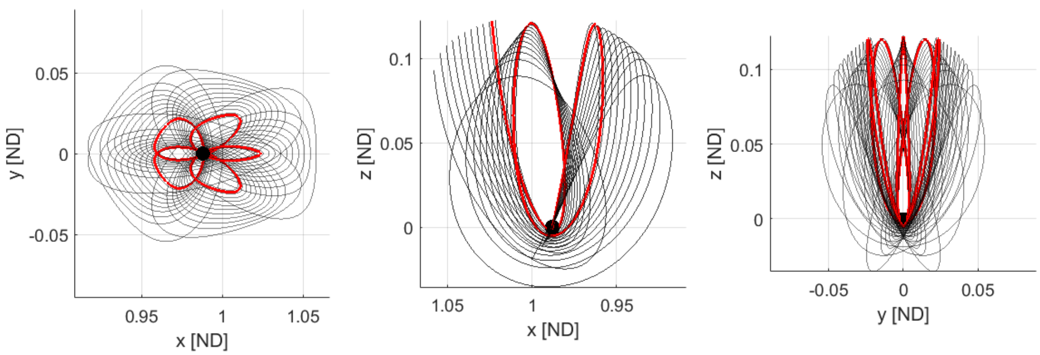


Fig. 15: $N_p = 5$ Tulip-shaped Orbit Family About $L_2$ (Red = Forked Solution from 1,800 km NRHO)

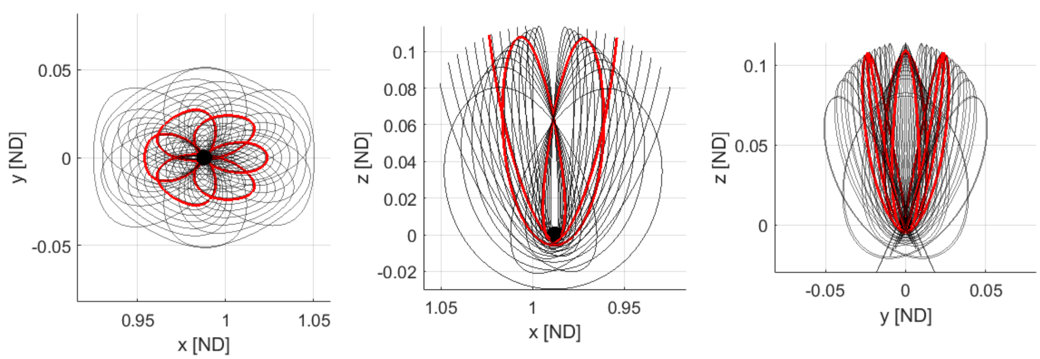


Fig. 16: $N_p = 6$ Tulip-shaped Orbit Family About $L_2$ (Red = Forked Solution from 1,800 km NRHO)

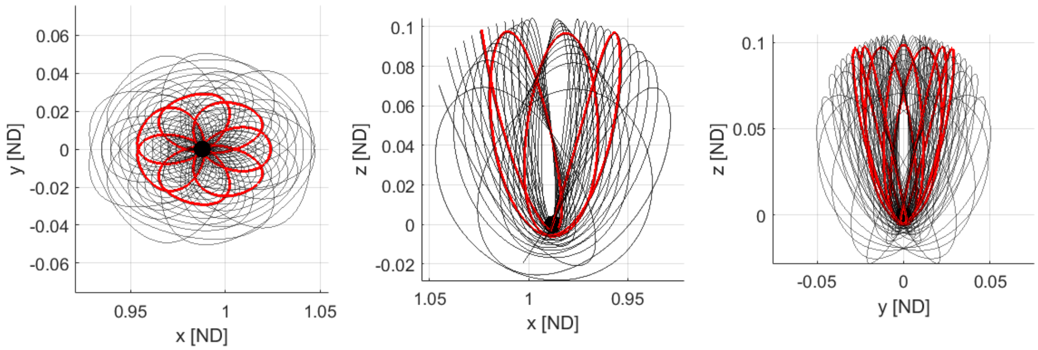


Fig. 17: $N_p = 7$ Tulip-shaped Orbit Family About $L_2$ (Red = Forked Solution from 1,800 km NRHO)

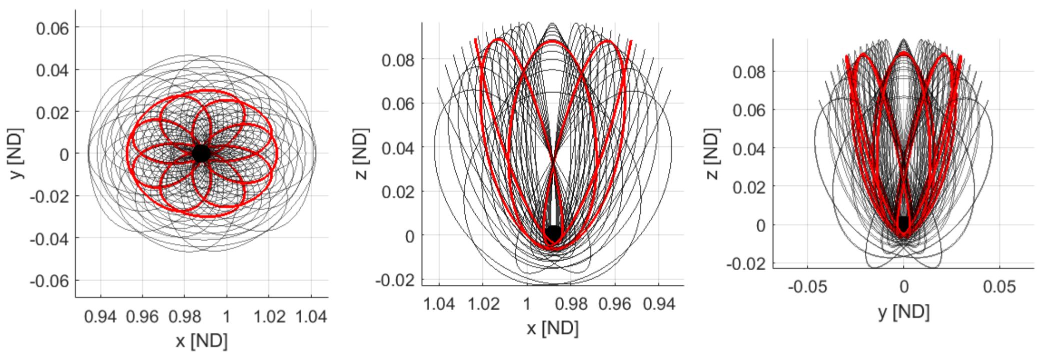


Fig. 18: $N_p = 8$ Tulip-shaped Orbit Family About $L_2$ (Red = Forked Solution from 1,800 km NRHO)

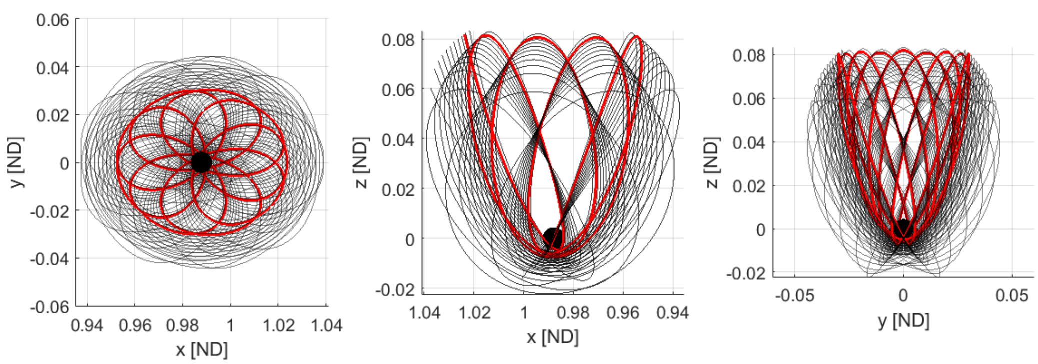


Fig. 19: $N_p = 9$ Tulip-shaped Orbit Family About $L_2$ (Red = Forked Solution from 1,800 km NRHO)

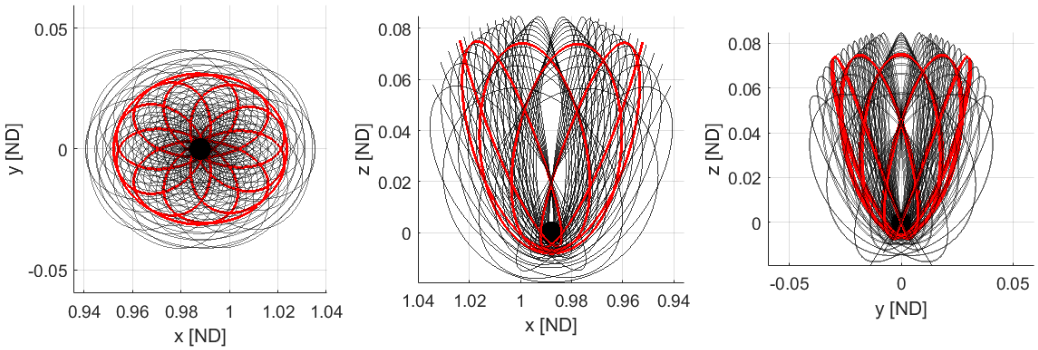


Fig. 20: $N_p = 10$ Tulip-shaped Orbit Family About $L_2$ (Red = Forked Solution from 1,800 km NRHO)

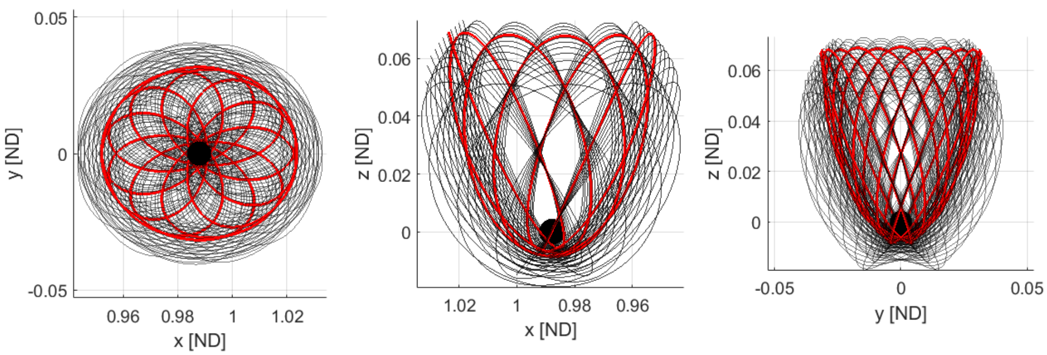


Fig. 21: $N_p = 11$ Tulip-shaped Orbit Family About $L_2$ (Red = Forked Solution from 1,800 km NRHO)

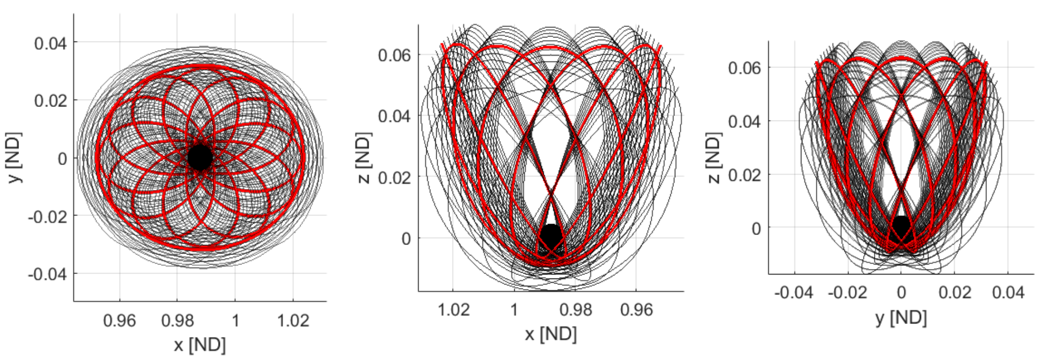


Fig. 22: $N_p = 12$ Tulip-shaped Orbit Family About $L_2$ (Red = Forked Solution from 1,800 km NRHO)

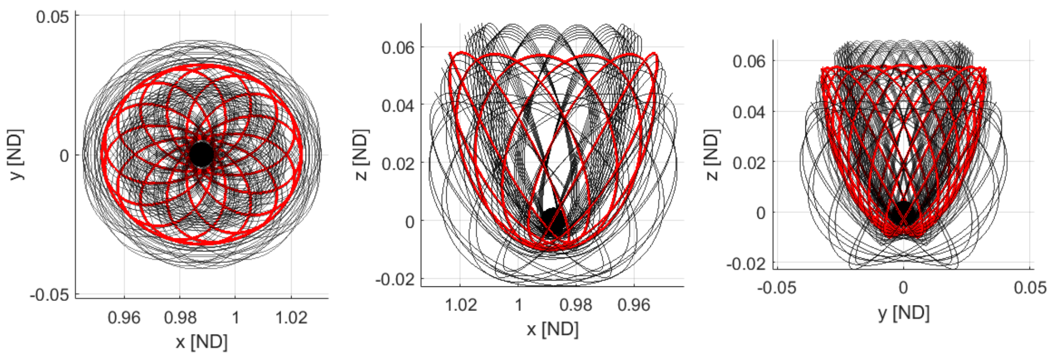


Fig. 23: $N_p = 13$ Tulip-shaped Orbit Family About $L_2$ (Red = Forked Solution from 1,800 km NRHO)

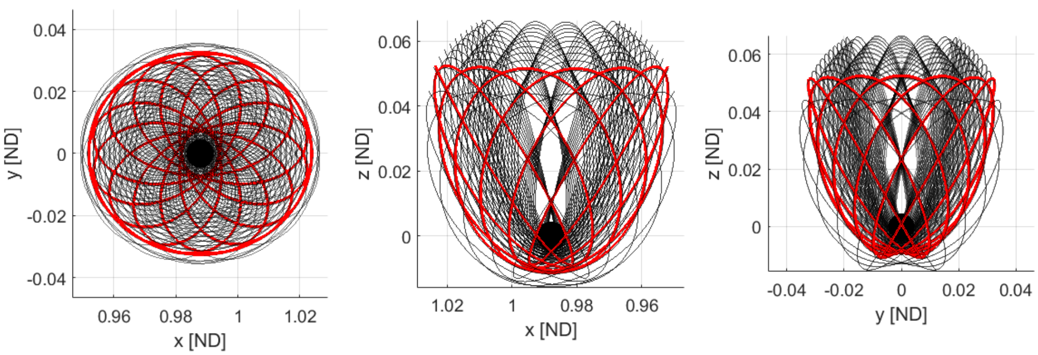


Fig. 24: $N_p = 14$ Tulip-shaped Orbit Family About $L_2$ (Red = Forked Solution from 1,800 km NRHO)

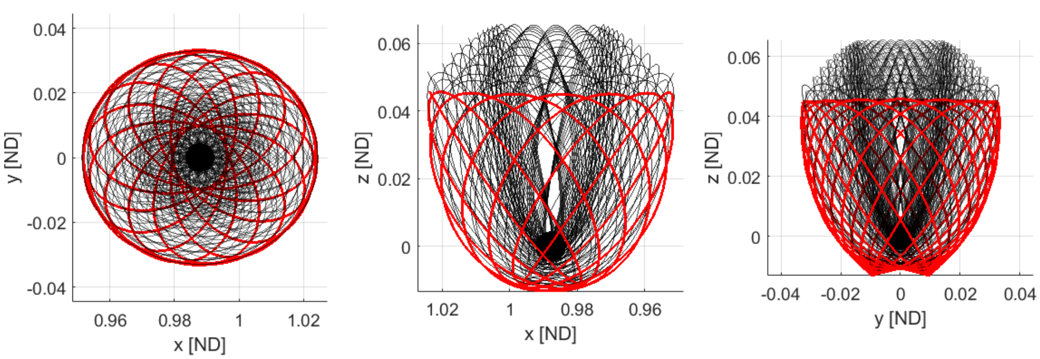


Fig. 25: $N_p = 15$ Tulip-shaped Orbit Family About $L_2$ (Red = Forked Solution from 1,800 km NRHO)